Supporting Information

Synergistic Ruthenium Single-Atom and Nanoparticles in Nickel as Cooperative Catalysts for the Alkaline Hydrogen Evolution Reaction

Name

Gaëlle Kalhil[a], Marie-Sophie Dias-Fernandes[b,c], Sumit Bawari[d], Linghui Li[a,b], Chiddharth Muthuraj[a], Florent Ducrozet[e], Minkyoung Kwak[f], Miguel Comesana-Hermo[a], Andrea Zitolo[c], Stephan N. Steinmann[d], Shannon W. Boettcher[f], Cédric Tard[b], Benedikt Lassalle-Kaiser[c], Marion Giraud[a]*, Jennifer Peron[a]*

Affiliation

[a] Université de Paris, CNRS, ITODYS, F-75013 Paris, France

[b] Laboratoire de Chimie Moléculaire (LCM), CNRS, École Polytechnique, Institut Polytechnique de Paris, 91120 Palaiseau, France

[c] Synchrotron SOLEIL, l'Orme des Merisiers, Départementale 128, 91190 Saint-Aubin, France

[d] CNRS, ENS de Lyon, UMR 5182, Laboratoire de Chimie, F69342, Lyon, France

[e] Sorbonne Université, Collège de France, CNRS, Laboratoire Chimie de la Matière Condensée de Paris (LCMCP), F-75005 Paris, France

[f] Department of Chemical & Biomolecular Engineering and Department of Chemistry, University of California, Berkeley, CA 94720, USA

*marion.giraud@u-paris.f; jennifer.peron@u-paris.fr

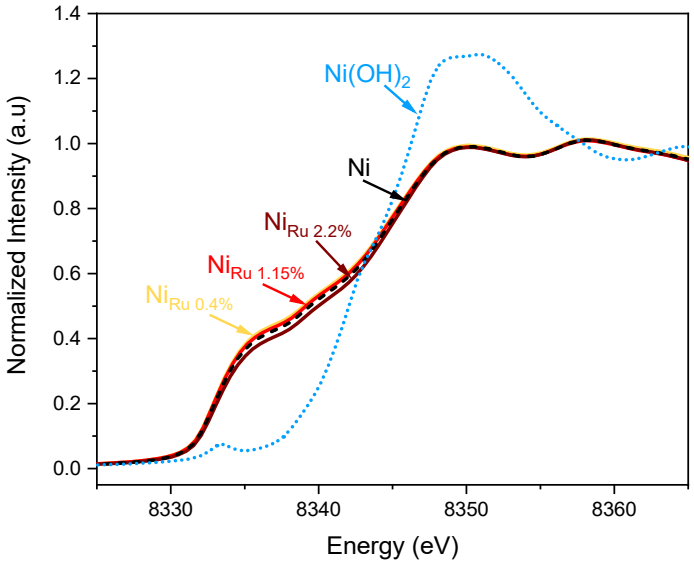

Figure S1: Ni K-edge XANES spectra of $Ni_{Ru\ 0.4\%}$, $Ni_{Ru\ 1.15\%}$, $Ni_{Ru\ 2.2\%}$, and reference Ni foil and $Ni(OH)_2$.

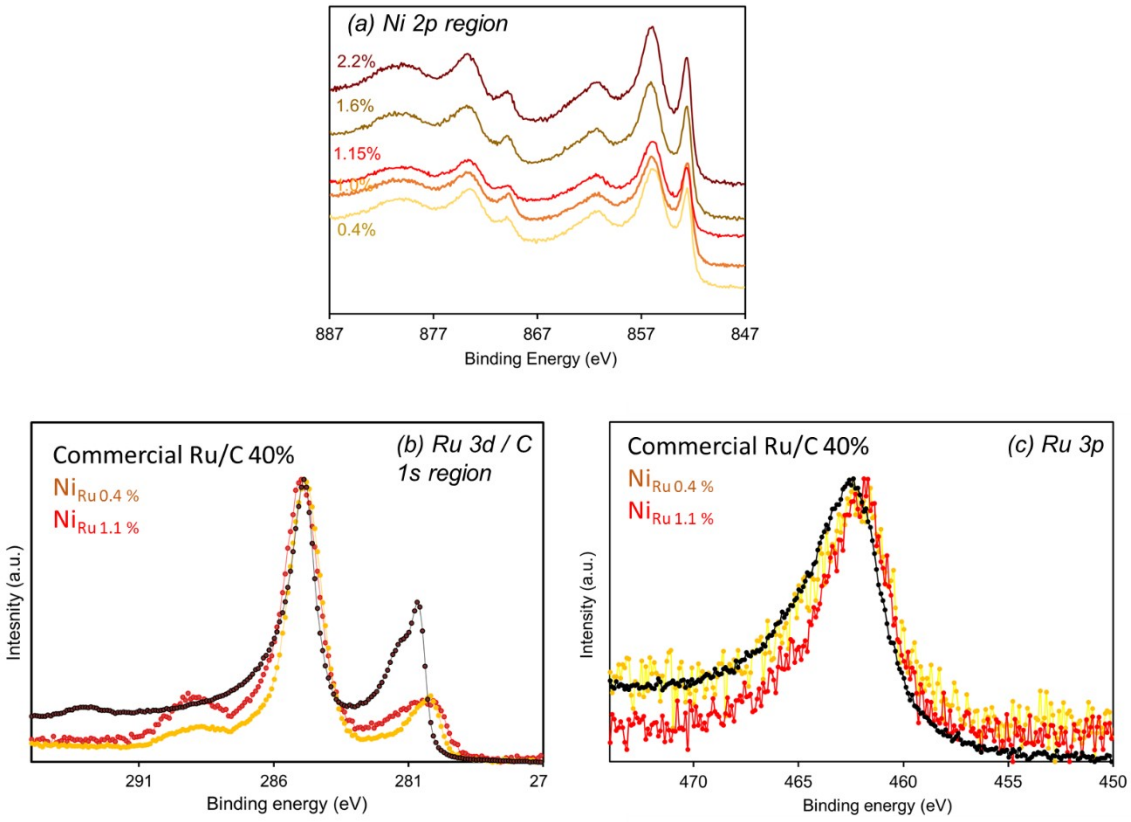

Figure S2: XPS in the (a) Ni 2p region. XPS spectra recorded in Ni 2p regions for the Ni_{Ru} particles. The XPS analysis in the Ni 2p region shows the presence of peaks characteristics of both Ni (0) with the 2p3/2 and 2p1/2 located at 852.7 and 970.1 eV, respectively, and Ni oxidized species with broad peaks

found at slightly higher binding energies. Ni particles are easily prone to oxidation upon exposure in air and humidity but, due to the overlapping of the peaks characteristic of the different phases of hydroxylated and oxidized Ni particles it is very difficult to propose an exact composition for the oxidized layer at the surface of the Ni particles. Nevertheless, we can state that the oxidized layer is sufficiently thin for metallic Ni to still be detected by XPS. **XPS in the Ru 3d/C 1s (b) and Ru 3p (c)** regions with signals normalized to the main peak intensity for comparison. These figures allow observing the shift of the Ru peak position towards lower binding energy in the composite material compared to commercial Ru/C particles.

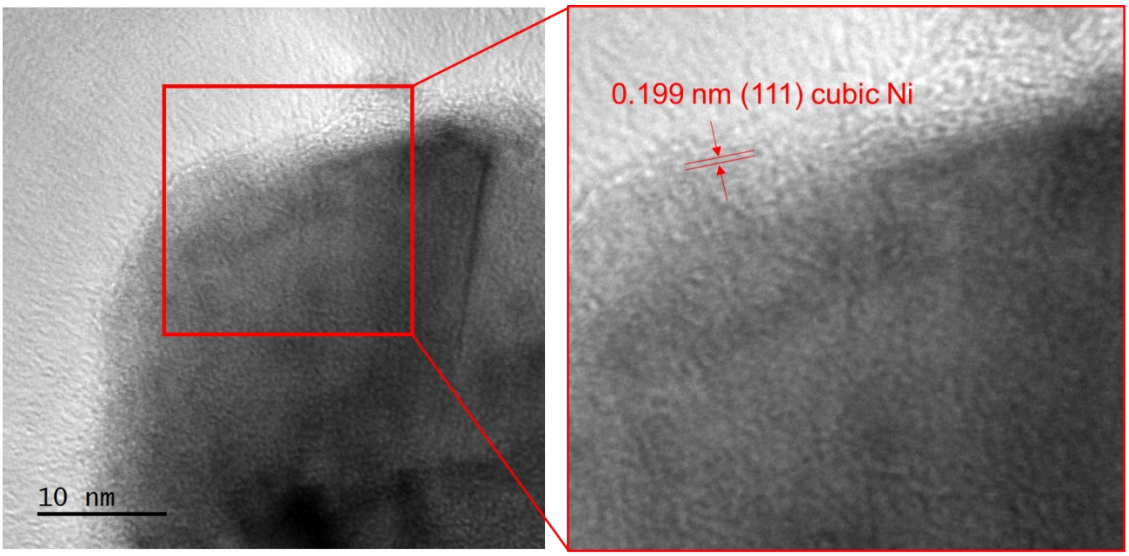

Figure S3: HRTEM images of NiRu 0.4, where no traces of Ru clusters of NPs can be found. The inset shows the crystalline lattice of Ni fcc.

Table S1. Structural parameters extracted from the Ru K-edge EXAFS fittings of the Ni_{Ru} catalysts.

Samples	Shell	CN	CN_{Tot} (metal shell)	R (Å)		σ^2 (Å^{-2})	ΔE^0 (eV)	R_f (%)
				XRD	EXAFS			
Ru foil	Ru-Ru	12	12	2.65	2.68	0.003	3.8	0.6
RuO_2	Ru-O	6		1.94	1.97	0.003	2.9	0.6
$Ni_{Ru(0.4\%)}$	Ru-Ni	8.6(±0.29)	8.6		2.50	0.0036	9.5	0.4
	Ru-O	0.9(±0.51)			1.90	0.003		
$Ni_{Ru(1\%)}$	Ru-Ru	5.1(±0.56)	11.3		2.64	0.007	9.2	0.3
	Ru-Ni	6.2(±0.51)			2.51	0.007		
	Ru-O	1.2(±0.29)			1.93	0.003		
$Ni_{Ru(1.15\%)}$	Ru-Ru	3.4(±0.40)	9.1		2.65	0.007	4.8	0.1
	Ru-Ni	5.7(±0.34)			2.51	0.007		
	Ru-O	1.6(±0.23)			1.95	0.003		
$Ni_{Ru(1.6\%)}$	Ru-Ru	6.0(±0.33)	10.3		2.63	0.007	11.9	0.1
	Ru-Ni	4.3(±0.24)			2.51	0.007		
	Ru-O	1.4(±0.15)			1.90	0.003		
$Ni_{Ru(2.2\%)}$	Ru-Ru	5.1(±0.45)	9.4		2.64	0.007	7.5	0.3
	Ru-Ni	4.3(±0.36)			2.52	0.007		
	Ru-O	1.4(±0.23)			1.95	0.003		
$Ni_{Ru(3.5\%)}$	Ru-Ru	5.4(±0.67)	9.5		2.63	0.007	11.9	0.6
	Ru-Ni	4.1(±0.52)			2.51	0.007		
	Ru-O	1.7(±0.32)			1.90	0.003		

CN is the coordination number, R the interatomic distance, σ^2 the Debye-Waller factor, ΔE^0 the inner potential correction, and R_f describes the goodness of the fit.

The coordination numbers of $Ni_{Ru\ 0.4\%}$ are about 8.6 for the Ru-Ni interaction and 0.9 for the Ru-O interaction, providing evidence that Ru atoms are linked to the Ni atoms. The absence of a Ru-Ru contribution confirms that the Ru atoms are dispersed within Ni particles as single atoms. With increasing Ru loading, the Ru-Ru average coordination number (CN) evolves from 0 (0.4 $Ni_{Ru\ 0.4\ wt.\%}$) to 3.4 ($Ni_{Ru\ 1.15\ wt.\%}$) and further to 5.1 ($Ni_{Ru\ 2.2\ wt.\%}$), indicating the formation of Ru nanoparticles. However, the Ru-Ni CN remains high for both $Ni_{Ru\ 1.15\ wt.\%}$ (5.7) and $Ni_{Ru\ 2.2\ wt.\%}$ (4.3), while the total coordination number (CN_{Tot}) is unchanged, revealing a modification of the chemical environment of the Ru atoms. These results are consistent with the coexistence of Ru single atoms (SAs) and Ru nanoparticles. At low Ru content, Ru SAs dominate over Ru nanoparticles, resulting in a higher Ru-Ni CN. Then, as the Ru loading increases, the Ru-Ni decreases and the Ru-Ru CN increases, reflecting the presence of an increased amount of Ru nanoparticles as compared to Ru SAs. This evolution has been previously observed in single-atom alloys dispersed in Ni particles, where the Ru-Ru CN increases from 0 (0.4 wt.% RuNi) to 2.2 (0.6 wt.% RuNi) and further to 6.7 (2 wt.% RuNi), with corresponding Ru-Ni CN of 5.4, 5.8 and 2.5, respectively.[1]

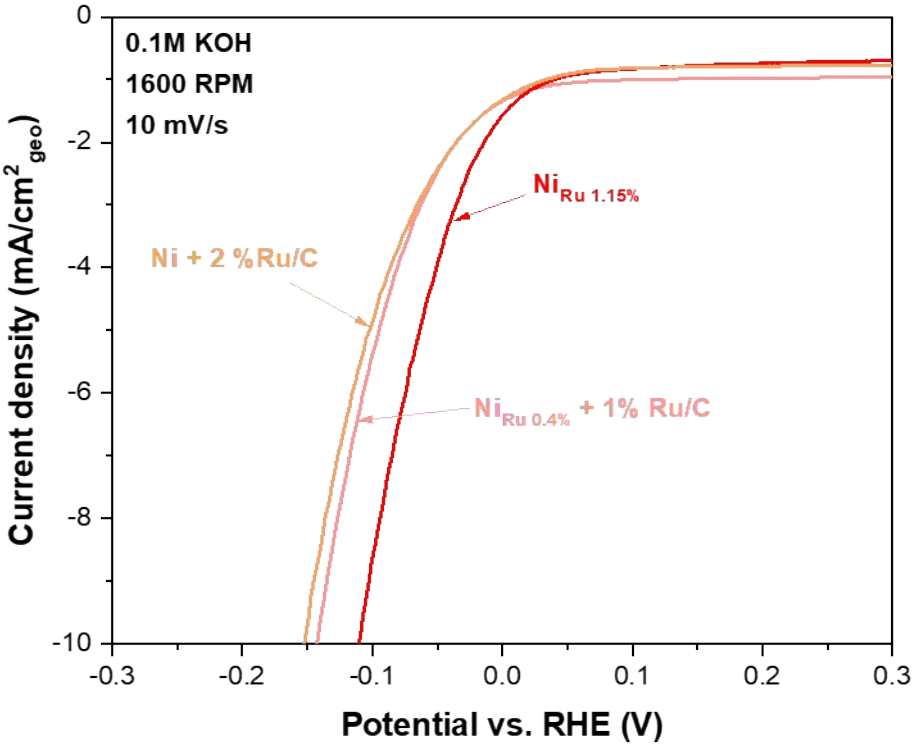

Figure S4 : LSV of Ni+2%Ru, $Ni_{Ru0.4\%}$ + 1% Ru, $Ni_{Ru1.15\%}$. LSV curves of commercial Ni + 2% Ru/C (mixture of pure Ni particles prepared in similar conditions as other materials and commercial Ru nanoparticles supported on C), $Ni_{Ru\ 0.4\%}$ + 1% Ru/C (mixture of $Ni_{Ru\ 0.4\%}$ i.e. atomically dispersed Ru atom in Ni particles obtained when using 0.4 wt.% of Ru mixed with commercial Ru nanoparticles supported on C), and $Ni_{Ru\ 1.15\%}$ (i.e. the composite material obtained and including SAA and nanoparticles) in 0.1M KOH. It should be noted that the total carbon content in the electrode was equal for all the experiments. The LSV analysis shows the higher catalytic activity when both Ru nanoparticles at the surface and atomically dispersed Ru single atom alloy coexist in the Ni-based material. These results highlight the synergistic effect between the Ni surface, Ru nanoparticles, and Ru single atom active sites.

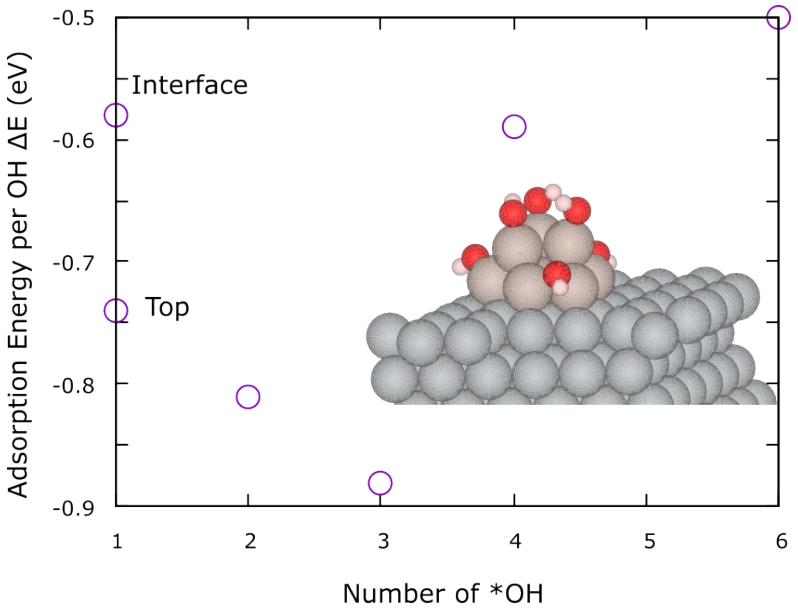

Figure S5. *OH Adsorption Energies for a covered nanoparticle. Differential adsorption energy for OH adsorption over the Ni-Ru-NP catalyst. Inset: structure of 6 *OH adsorbed on Ni-Ru-NP, O (red), H (white).

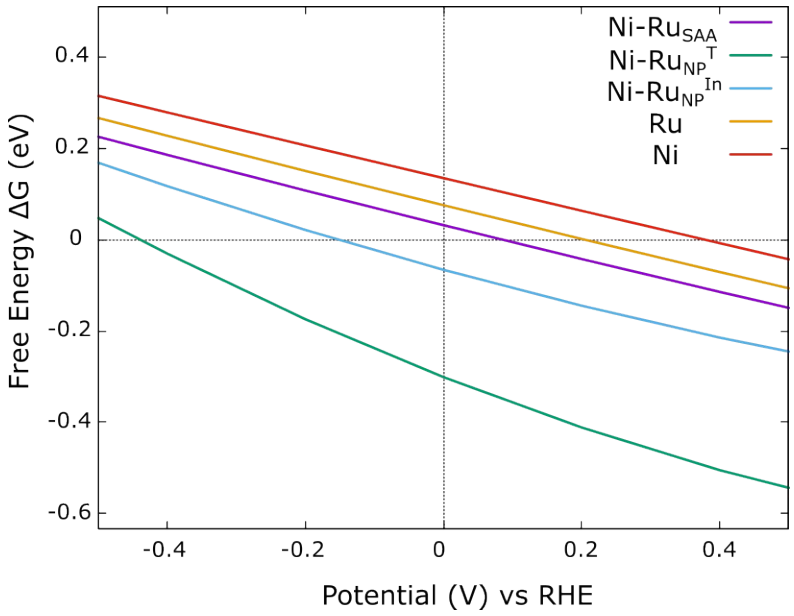

Figure S6. Free Energy of Water binding. Potential-dependent Gibbs free energy of water adsorption (*H_2O) at pH 14 for different surface sites.

Table S2: Water dissociation energies of different active sites

Active site		Water dissociation energy (ΔE) eV $*H_2O \rightarrow *H + *OH$
Ni		-0.37
Ru		-0.53
Ni-Ru-SAA		-0.22
Ni-Ru-NP	**Top**	-0.36
	Interface	-0.63

1. Liu, W.; Feng, H.; Yang, Y.; Niu, Y.; Wang, L.; Yin, P.; Hong, S.; Zhang, B.; Zhang, X.; Wei, M., Highly-efficient RuNi single-atom alloy catalysts toward chemoselective hydrogenation of nitroarenes. *Nature Communications* **2022,** *13* (1), 3188.